Journal of Materials Chemistry A

ROYAL SOCIETY OF CHEMISTRY

PAPER

View Article Online
View Journal | View Issue

Cite this: J. Mater. Chem. A, 2025, 13, 4197

High-output, thermally resilient Nano-TiO_2 dielectric gel triboelectric nanogenerator for energy harvesting and reliable temperature-independent pressure sensing†

Hyosik Park, ‡[a] Yeonkyeong Ryu,‡[a] Hyeonseo Joo,[a] Sujeong Gwak,[a] Gerald Selasie Gbadam,[a] Simiao Niu [b] and Ju-Hyuck Lee *[ac]

In triboelectric nanogenerators (TENGs), polymers are widely utilized, with plasticizers serving essential roles in industrial polymer applications. Plasticized polyvinyl chloride (PVC) dielectric gel TENGs are particularly effective at generating high outputs due to their strong triboelectric properties. However, elevated temperatures can cause plasticizer leakage due to weak interactions with the polymer matrix, reducing the TENG's stability. This study addresses these limitations by incorporating titanium dioxide nanoparticles (TiO_2 NPs) into a dielectric gel, achieving significantly enhanced dielectric properties and thermal stability. The TiO_2 NPs increase the dielectric constant, reduce leakage current, and improve output performance to 121 V, 11.1 μA, and 149 μW cm^{-2}. Additionally, interactions between TiO_2 NPs and polar components of the plasticizers prevent leakage, ensuring stability at high temperatures. The resulting nano-TiO_2 dielectric gel TENG demonstrates superior mechanical and thermal resilience, enabling reliable operation in diverse environments. Furthermore, it features a temperature-independent pressure sensor with consistent sensitivity (S = 2.03 V kPa^{-1} for 10–40 kPa and S = 0.97 V kPa^{-1} for 40–100 kPa) and accuracy over a wide temperature range (25 °C to 55 °C). These properties make the nano-TiO_2 dielectric gel TENG ideal for sustainable energy harvesting and temperature-robust sensing applications, enhancing the practical utility of TENGs across variable climates.

Received 5th November 2024
Accepted 8th January 2025

DOI: 10.1039/d4ta07867e

rsc.li/materials-a

1. Introduction

Energy harvesting technology is gaining considerable attention as a sustainable energy solution to address the ongoing energy crisis and mitigate climate change. The growing demand for energy, driven by the increasing use of personal electronic devices and components for Internet of Things (IoT) platforms, further underscores the need for innovative energy sources. Various energy harvesting technologies exist, including piezoelectric nanogenerators,[1–3] pyroelectric nanogenerators,[4–6] and hydrovoltaic nanogenerators.[7–9] Among them, triboelectric nanogenerators (TENGs) stand out as mechanical energy harvesting devices that utilize contact electrification and electrostatic induction effects.[10–12] TENGs have garnered significant interest due to their high energy conversion efficiency, high output voltage, simple manufacturing process, and low cost. Additionally, they are being actively explored for diverse applications such as electronic skin,[13,14] wearable devices,[15,16] and self-powered sensors.[17,18]

Among these applications, TENG-based self-powered pressure sensors utilizing biodegradable polymers,[19,20] stretchable polymers,[21,22] and ionic polymers[23,24] have demonstrated significant potential for converting mechanical pressure into electrical signals.[25,26] High-output TENGs are particularly desirable for pressure sensors, as higher output leads to greater sensitivity, enabling the detection of finer pressure changes with increased accuracy. However, a key limitation of TENG-based pressure sensors is that their output performance often fluctuates with temperature, which can affect the accuracy of pressure measurements. Changes in temperature can cause variations in triboelectric output, leading to inconsistent sensor readings and reduced reliability, especially in environments with fluctuating temperatures.[27,28] Therefore, developing temperature-independent pressure sensors that maintain

[a]Department of Energy Science and Engineering, DGIST, 333, Techno Jungang-daero, Hyeonpung-eup, Dalseong-gun, Daegu, 42988, Republic of Korea. E-mail: jhlee85@dgist.ac.kr

[b]Department of Biomedical Engineering, Rutgers University, Piscataway, NJ 08854, USA

[c]Energy Science and Engineering Research Center, Daegu Gyeongbuk Institute of Science and Technology (DGIST), 333 Techno Jungang-daero, Hyeonpung-eup, Dalseong-gun, Daegu 42988, Republic of Korea

† Electronic supplementary information (ESI) available. See DOI: https://doi.org/10.1039/d4ta07867e

‡ The authors contributed equally to this work.

consistent performance across different temperatures is critical for ensuring reliable operation in a wide range of environments.

Polyvinyl chloride (PVC) gel-based TENGs have been identified as suitable candidates for high-sensitivity pressure sensors due to their deformability, high tribo-negativity, and high dielectric constant, which together allow them to generate high output.[15] However, the dielectric gel-based TENGs can suffer from performance degradation at elevated temperatures due to poor thermal stability. Titanium dioxide nanoparticles (TiO_2 NPs) are renowned for their excellent physical and thermal stability, high permittivity, photocatalytic properties, and tribo-positive properties.[29,30] Their large specific surface area and highly reactive unsaturated surface atoms enable strong interactions with the polar components of plasticizers, enhancing the thermal stability of the dielectric gel by preventing plasticizer leakage.[31] By doping TiO_2 NPs into the dielectric gel, it is possible to develop a temperature-independent pressure sensor.

In this study, we incorporated TiO_2 NPs into PVC gel to enhance the thermal stability of TENGs and develop a temperature-independent pressure sensor. Although the incorporation of TiO_2 NPs imparts tribo-positive properties to the nano-TiO_2 dielectric gel, it significantly enhances the dielectric constant and reduces leakage current. These advantages outweigh the potential drawbacks of increased tribo-positivity, resulting in superior output performance (121 V, 11.1 μA, 149 μW cm^{-2}) and improved thermal stability. This enhanced thermal stability allows the pressure sensor to maintain consistent sensitivity across a wide temperature range (25 °C to 55 °C), with stable sensitivity in both low-pressure (2.03 V kPa^{-1} @ 10–40 kPa) and high-pressure (0.97 V kPa^{-1} @ 40–100 kPa) ranges, independent of temperature variations. By overcoming the limitations of traditional TENG-based sensors, this innovation ensures reliable performance across diverse climates, making the nano-TiO_2 dielectric gel TENG ideal for sustainable energy harvesting and precise pressure sensing in a wide range of fluctuating environmental conditions.

2. Experimental section

2.1 Materials

The nano-TiO_2 dielectric gel was prepared using commercial PVC powder (Mw 275 000; Scientific Polymer Products, Inc., USA) and mixed TiO_2 nano powder (anatase 80% and rutile 20%, 21 nm particle size, ≥99.5% trace metals basis; Sigma-Aldrich) with tetrahydrofuran (THF 99.5%; DAEJUNG, Korea) as the solvent and DBA (TCI, Japan) as plasticizers.

2.2 Fabrication of PVC gel and nano-TiO_2 dielectric gels

PVC powder was dissolved in THF, and DBA was added to the solution, which was stirred for 24 hours at 200 rpm. The ratio of PVC to the DBA plasticizer was 1 : 3. TiO_2 nanoparticles were dispersed in THF using a vortex mixer and sonication. This nanoparticle dispersion was then added to the PVC gel solution. The resulting mixture was stirred under the same conditions and sonicated for 1 hour. The solution was then poured into a glass dish to allow THF to evaporate at room temperature (24 °C) over two days, resulting in a soft, gel-like dielectric elastomer.

2.3 Fabrication of temperature-independent pressure sensing applications

The bottom part of the pressure sensor consists of nine 2 cm × 2 cm Al electrodes mounted on a glass substrate and interconnected with wires. A 2 cm × 2 cm piece of PVC gel or nano-TiO_2 dielectric gel is securely fixed above each electrode. The top part of the sensor is designed to be either a plus sign or a square shape. It comprises a 2 cm × 2 cm Al electrode attached to another glass substrate, with a 2 cm × 2 cm nylon film adhered to it.

2.4 Characterization of PVC gel and nano-TiO_2 dielectric gels

Surface and cross-sectional images, as well as energy-dispersive spectroscopy (EDS) images, were obtained using a scanning electron microscope (SEM, Hitachi, S-4800). An X-ray diffractometer (Rigaku, MiniFlex 600) with Cu Kα radiation ($\lambda = 1.5418$ Å) was used to determine the crystalline properties of the samples. The chemical structures of the specimens were analyzed using a Fourier transform infrared (FT-IR) spectrometer (Spectrometer 100; PerkinElmer, USA). The mechanical properties of the PVC gel and nano-TiO_2 dielectric gels were evaluated using a universal testing machine (UTM, ST-1000; SALT, Co. LTD., Korea) according to ASTM D638 (type V), with a crosshead speed of 50 mm min^{-1} at room temperature (23 °C). Uniaxial tensile tests were conducted on dumbbell-shaped specimens cut from flat, drop-cast films with a thickness of 0.4 mm. The dielectric properties of the PVC gel and nano-TiO_2 dielectric gels were measured over a frequency range of 1 Hz to 10 kHz with a signal amplitude of 1 V using an LCR meter (IM3533; HIOKI, Japan) at room temperature (25 °C). Leakage current was measured using a source meter (Keithley 2450; Keithley Instruments, USA) under an applied electric field of 80 V mm^{-1} at room temperature (25 °C) with a dielectric gel area of 1 cm^2. Surface potential measurements were performed using Kelvin probe force microscopy (KPFM, XE-100; Park Systems, Korea) with a Pt/Cr-coated silicon tip and a lock-in amplifier. Plasticizer weight loss was calculated after each 24 hour annealing period at 55 °C in an oven for 7 days. Additionally, glass transition temperatures (T_g) were measured using differential scanning calorimetry (DSC, 131 EVO; SETARAM, Switzerland).

2.5 Measurements: TENG output and temperature-independent pressure sensing

The output performance of the TENG was measured in an active area of 2 cm × 2 cm (contact material: nylon). Open-circuit voltages (V_{OC}) and short-circuit currents (I_{SC}) were measured using an electrometer (Model 6514; Keithley Instruments, Inc., USA). The cyclic contact-separation process was carried out using a shaker (ET-139; Labworks Inc., USA), a function generator (33210A; KEYSIGHT, USA), and a linear power amplifier (PA-138; Labworks Inc., USA). Additionally, the TENG output

performance was measured at different temperatures (25 °C, 35 °C, 45 °C, and 55 °C) and pressures.

3. Results and discussion

3.1 Intermolecular interactions and structural analysis of nano-TiO_2 dielectric gels

The nano-TiO_2 dielectric gel was synthesized by incorporating various concentrations of TiO_2 NPs into a dibutyl adipate (DBA)-lasticized PVC gel, as detailed in the Experimental Section and illustrated in Fig. S1.† The intermolecular interactions in the PVC gel and nano-TiO_2 dielectric gel are shown in Fig. 1a, indicating that the PVC chains interact with the TiO_2 NPs *via* dipole–dipole forces between the chlorine (Cl) atoms in PVC and the titanium (Ti) atoms in TiO_2 NPs. Additionally, interactions occur between the TiO_2 NPs and the carbonyl (C=O) groups in DBA, enhancing the structural stability of the nano-TiO_2 dielectric gel network. Photographs, scanning electron microscopy (SEM) images, and energy-dispersive spectroscopy (EDS) of the PVC gel and nano-TiO_2 dielectric gel are shown in Fig. 1b, S2 and S3.† The PVC gel is transparent with a smooth surface, whereas the nano-TiO_2 dielectric gel is opaque and rough with numerous TiO_2 NPs dispersed throughout the composite gel. The corresponding EDS images indicate that the TiO_2 NPs are evenly dispersed in the TiO_2 dielectric gel (Ti: 1.13 at%). Fig. 1c shows the X-ray diffraction (XRD) peaks of TiO_2 dielectric gel as a function of TiO_2 NPs concentration. The crystalline peak of PVC appears at 20°, and the peak intensity increases with higher concentrations of TiO_2 NPs, indicating that the amorphous region, caused by the plasticizer, expands as TiO_2 NPs combine with the plasticizer. Representative peaks of mixed-phase TiO_2 NPs (80% anatase (A) and 20% rutile (R)) are observed at 25° (A:101), 37° (A:004), and 47° (A:200), with prominent TiO_2 NPs peaks clearly visible in the 5 wt% TiO_2 dielectric gel.[32] The high anatase content in the mixed-phase TiO_2 enables photocatalytic properties, which can be utilized for self-cleaning under sunlight (Fig. S4†). This self-cleaning ability prevents the reduction caused by contaminants on the triboelectric layer.

Fig. 1d shows Fourier transform infrared spectroscopy (FT-IR) spectra of the TiO_2 dielectric gel, demonstrating the interaction between TiO_2 NPs and the DBA plasticizer when the DBA is physically dispersed within the PVC chain. In the PVC gel, the C=O peak of the DBA plasticizer appears sharply at 1728 cm^{-1}. As the concentration of TiO_2 increases, this peak broadens, reflecting stronger interactions between the TiO_2 NPs and the DBA plasticizer.[33] These characteristics are further evidenced by the stress–strain curve, which demonstrates improved mechanical properties of the TiO_2 dielectric gel with increasing concentrations of TiO_2 nanoparticles (Fig. 1e). Nano-TiO_2 not only interacts with PVC chains and plasticizers but also remains fixed under strain, limiting the mobility of PVC chains and plasticizers while creating physical crosslinking points through entanglement.[34] This mechanism explains the observed

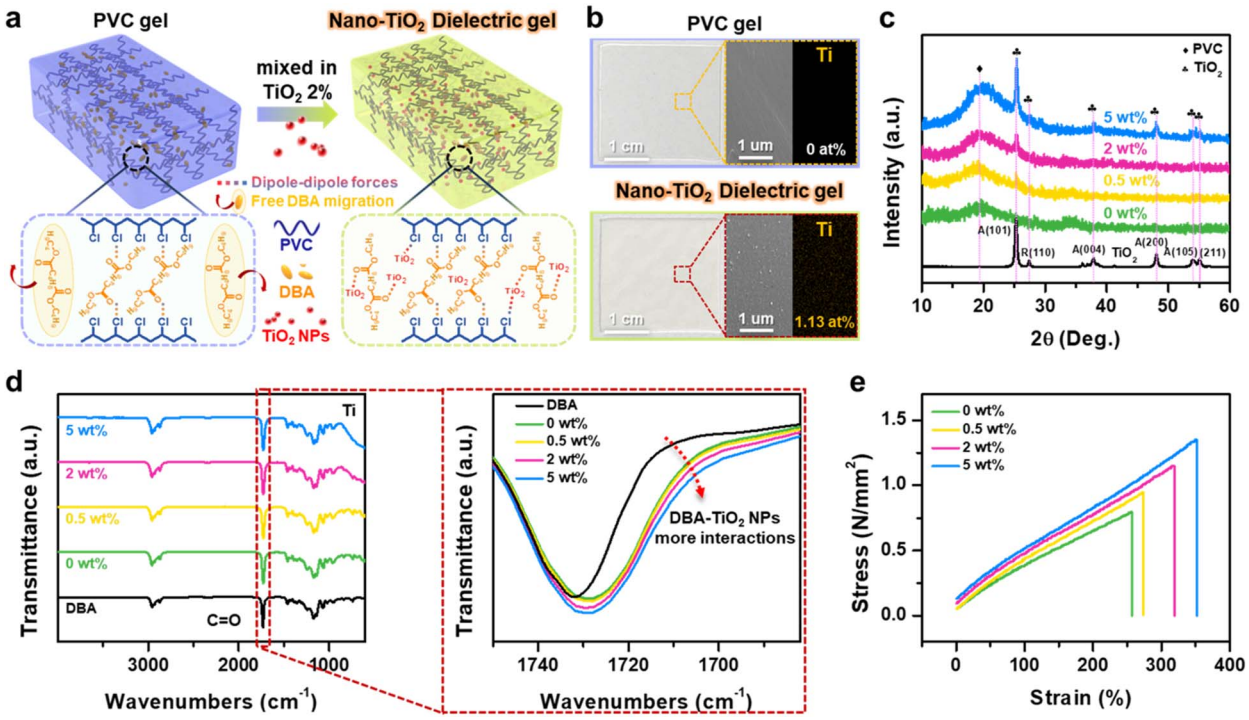

Fig. 1 Intermolecular structures and characteristics of PVC gel and nano-TiO_2 dielectric gels. (a) Schematic of PVC gel and 2 wt% TiO_2 dielectric gel intermolecular structures and forces. (b) Comparison of photographs and SEM-EDS images of PVC gel and 2 wt% TiO_2 dielectric gel. (c) XRD patterns showing crystalline structures of TiO_2 nanoparticle and TiO_2 dielectric gels across a range of TiO_2 concentrations from 0 to 5 wt%. (d) FT-IR spectra of DBA and TiO_2 dielectric gels with varying TiO_2 NPs concentrations from 0 to 5 wt%. (e) Stress–strain curves of the TiO_2 dielectric gels with TiO_2 NPs concentrations ranging from 0 to 5 wt%.

increase in Young's modulus as the TiO_2 concentration rises. Specifically, both the elongation at break and Young's modulus increase as the concentration of TiO2 NPs increases (Fig. S5†).

3.2 Evaluation of output performance in nano-TiO_2 dielectric gel TENG

Fig. 2a shows the schematic and working principles of the TiO_2 dielectric gel-based TENG. The top layer of the TENG consists of a nylon/Al electrode, while the bottom layer is composed of a TiO_2 dielectric gel/indium tin oxide (ITO) electrode. The TENG operates based on the combined effects of contact electrification and electrostatic forces. When external pressure is applied, the nylon and TiO_2 dielectric gel come into contact, causing the nylon to become positively charged and the TiO_2 dielectric gel to become negatively charged due to its triboelectric properties. As the top layer moves away from the bottom, the negative charges on the TiO_2 dielectric gel surface repel electrons, forcing them to flow from the bottom electrode to the top electrode through external circuits.

We quantitatively evaluated the output performance (peak-to-peak voltage and current) of TENGs made from both PVC gel and TiO_2 dielectric gels with various concentrations of TiO_2 (from 0 wt% to 5 wt%) under a contact-separation pressure of 20 N and a frequency of 2 Hz. The TENG made from PVC gel produced an output voltage of 99.8 V and a current of 9.6 μA (Fig. 2b). This serves as the baseline for assessing the impact of TiO_2 doping. With the incorporation of 0.5 wt% TiO_2 into the PVC gel, the output increased to 102 V and 10 μA, indicating that the concentration of TiO_2 NPs positively correlates with higher output. The maximum output values were observed at 2 wt% TiO_2, reaching 121 V and 11.1 μA, representing a 20% improvement compared to the PVC gel. However, increasing the TiO_2 concentration to 5 wt% resulted in a decrease in output, down to 92 V and 8.6 μA. We used the 2 wt% TiO_2 dielectric gel, which exhibited the highest output, to investigate TENG

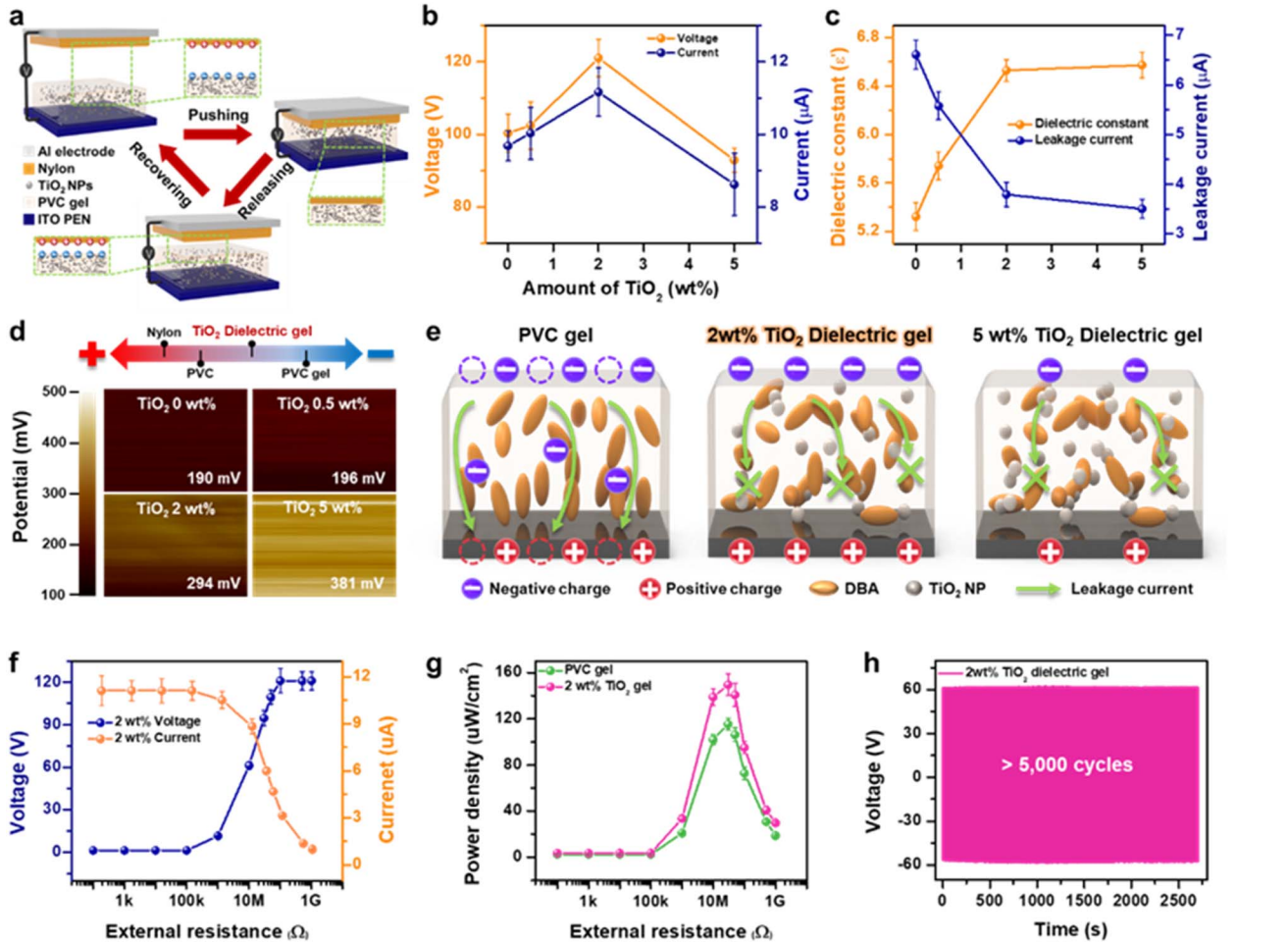

Fig. 2 Output performance of nano-TiO_2 dielectric gel-based TENG. (a) Schematic of device structure and working principle of TiO_2 dielectric gel TENG. (b) Output voltage and current in TENGs with different TiO_2 NPs concentrations (0 wt% to 5 wt%). (c) Dielectric constant and leakage current of TiO_2 dielectric gels across a range of TiO_2 concentrations (0 wt% to 5 wt%). (d) Surface potential of TiO_2 dielectric gels and comparison of triboelectricity with other polymers (nylon and PVC). (e) Schematic of the induced surface charges and leakage current based on different concentration of TiO_2 NPs. (f) Output voltage and current based 2 wt% TiO_2 dielectric gel TENG with external load resistances. (g) Power density of the PVC gel and 2 wt% TiO_2 dielectric gel-based TENG with external load resistances. (h) Durability test of the 2 wt% TiO_2 dielectric gel-based TENG for more than 5000 cycles.

behavior under different pressures and frequencies (Fig. S6 and S7†). We also compared the TENG output performance of mixed-phase and rutile-phase TiO_2 dielectric gels, finding that the mixed-phase TiO_2 dielectric gel produced superior output, as discussed in detail in ESI Note S1 (Fig. S8†).

The triboelectric output is proportional to the surface charge density of the dielectric materials, and the induced surface charge density (σ') can be expressed by the following equation:[35]

$$\sigma' = \frac{\sigma x(t)}{\frac{d_{TiO_2\ \text{dielectric gel}}}{\varepsilon_{TiO_2\ \text{dielectric gel}}} + \frac{d_{\text{Nylon}}}{\varepsilon_{\text{Nylon}}} + x(t)} \quad (1)$$

where σ is the triboelectric charge density, and $\varepsilon_{TiO_2\ \text{dielectric gel}}$, $\varepsilon_{\text{Nylon}}$ are the permittivities of TiO_2 dielectric and nylon, and $d_{TiO_2\ \text{dielectric gel}}$, d_{Nylon} represent their thickness. $x(t)$ is the gap distance between the top and bottom layers. Fig. 2c illustrates the dielectric constant and leakage current of the TiO_2 dielectric gel, measured at a frequency of 100 kHz. The dielectric constant of the PVC gel was 5.3, which increased with the TiO_2 concentration: 5.7 at 0.5 wt%, 6.52 at 2 wt%, and 6.57 at 5 wt%. This rise in the dielectric constant contributed to the enhanced output of the TiO_2 dielectric TENG. Additionally, an increase in dielectric constant and loss was observed across all frequency ranges (Fig. S9†). The total induced charge density (σ_T) can decrease when charges dissipate quickly due to leakage paths, as described by:

$$\sigma_T = \sigma' - \sigma_D \quad (2)$$

where σ_T is the total charge density, and σ_D is the dissipation charge density. PVC gel exhibited the highest leakage current at 6.61 μA, leading to rapid charge dissipation. As the TiO_2 concentration increased, the dissipated charge decreased: 4.03 μA at 0.5 wt%, 2.45 μA at 2 wt%, and 2.29 μA at 5 wt%. Therefore, the combination of a higher dielectric constant and lower leakage current led to improved output up to 2 wt% TiO_2 NPs. In addition to dielectric constant and leakage current, TENG output is also influenced by the effective work function of the dielectric materials. To investigate this, the effective work functions of PVC gel and TiO_2 dielectric gels were measured using Kelvin probe force microscopy (KPFM) (Fig. 2d). The potential of the PVC gel was 190 mV. As the TiO_2 NP concentration increased, a shift toward more positive triboelectric properties was observed: 196 mV at 0.5 wt%, 294 mV at 2 wt%, and 381 mV at 5 wt%, indicating increased positive triboelectric potential with higher TiO_2 concentrations.[36] Fig. 2e compares the surface charge density of PVC gel, 2 wt%, and 5 wt% TiO_2 dielectric gel. For the PVC gel, the difference in work function resulted in a significant amount of charge, which dissipated quickly due to the high leakage current. At 5 wt% TiO_2, the TENG's output was primarily influenced by the effective work function rather than the dielectric constant or leakage current. This reduction in output at 5 wt% is attributed to a smaller difference in the effective work function between TiO_2 dielectric gel and nylon, suggesting the critical role of the effective work function in determining TENG performance. Conversely, the 2 wt% TiO_2 dielectric gel achieved maximum output due to an optimized balance of dielectric constant, reduced leakage current, and effective work function. Moreover, we also explored the relationship between compatibility and performance by incorporating a coupling agent into the optimized 2 wt% TiO_2 dielectric gel (Fig. S10†).[37,38] Although the coupling agent enhanced the compatibility between TiO_2 and PVC, it ultimately reduced TENG performance, as discussed in detail in ESI Note S2.†

To further evaluate the performance of the optimized 2 wt% TiO_2 dielectric gel TENG, the output voltage, current, and power density were measured under varying external load resistances (100 Ω to 1 GΩ), as shown in Fig. 2f and g. The maximum output power density was 141 μW cm^{-2} at 30 MΩ. Additionally, the output voltage remained stable, showing no significant degradation over 5000 cycles of repeated contact-separation motion of the TENG with a nylon film (Fig. 2h). To further assess the stability of the TiO_2 dielectric gel, potential plasticizer leakage under continuous friction was evaluated using SEM analysis of the counter material, nylon, both before and after the stability test (Fig. S11†). The results showed no noticeable changes on the nylon surface, confirming the material's stability.

3.3 Temperature-independent output performance of nano-TiO_2 dielectric gel TENG

To extend the operational range of TENGs, it is crucial that they maintain reliable energy harvesting capabilities under elevated thermal conditions. As discussed in Fig. 1, the incorporation of TiO_2 nanoparticles (NPs) into the PVC gel significantly enhances its thermal stability. Fig. 3a shows the performance of TENGs based on PVC gel and 2 wt% TiO_2 dielectric gel when subjected to a temperature range of 25 °C to 55 °C. The output from the PVC gel TENG decreased progressively from 25 °C to 55 °C, confirming its thermal instability (Fig. 3b and c). In contrast, the 2 wt% TiO_2 dielectric gel maintained consistent output across the same temperature range, demonstrating the effectiveness of TiO_2 doping in improving thermal resilience (Fig. 3d and e). The output voltage and current for 0.5 wt% and 5 wt% TiO_2 dielectric gel TENGs at different temperatures are shown in Fig. S12 and S13.† Additionally, Fig. 3f and g present the rate of change in output for TiO_2 dielectric gels with varying TiO_2 concentrations under thermal stress from 25 °C to 55 °C. TENGs based on lower TiO_2 concentrations (0 wt% and 0.5 wt%) exhibited reduced performance at elevated temperatures, whereas higher concentrations (2 wt% and 5 wt%) displayed stable outputs, unaffected by temperature fluctuations. We further examined the impact of dielectric constants and leakage currents on the output performance of TiO_2 dielectric gel TENGs across the temperature range of 25 °C to 55 °C in Fig. 3h. While the dielectric constants of PVC gel and TiO_2 dielectric gels remained relatively stable across the range of temperatures and TiO_2 NP concentrations, the leakage currents were highly sensitive to these variables. Specifically, the leakage current of the PVC gel increased significantly from its initial value at room temperature to higher values at 55 °C. In contrast, the 2 wt% and 5 wt% TiO_2 dielectric gels exhibited only minimal increases in leakage current. The decrease in output performance at lower

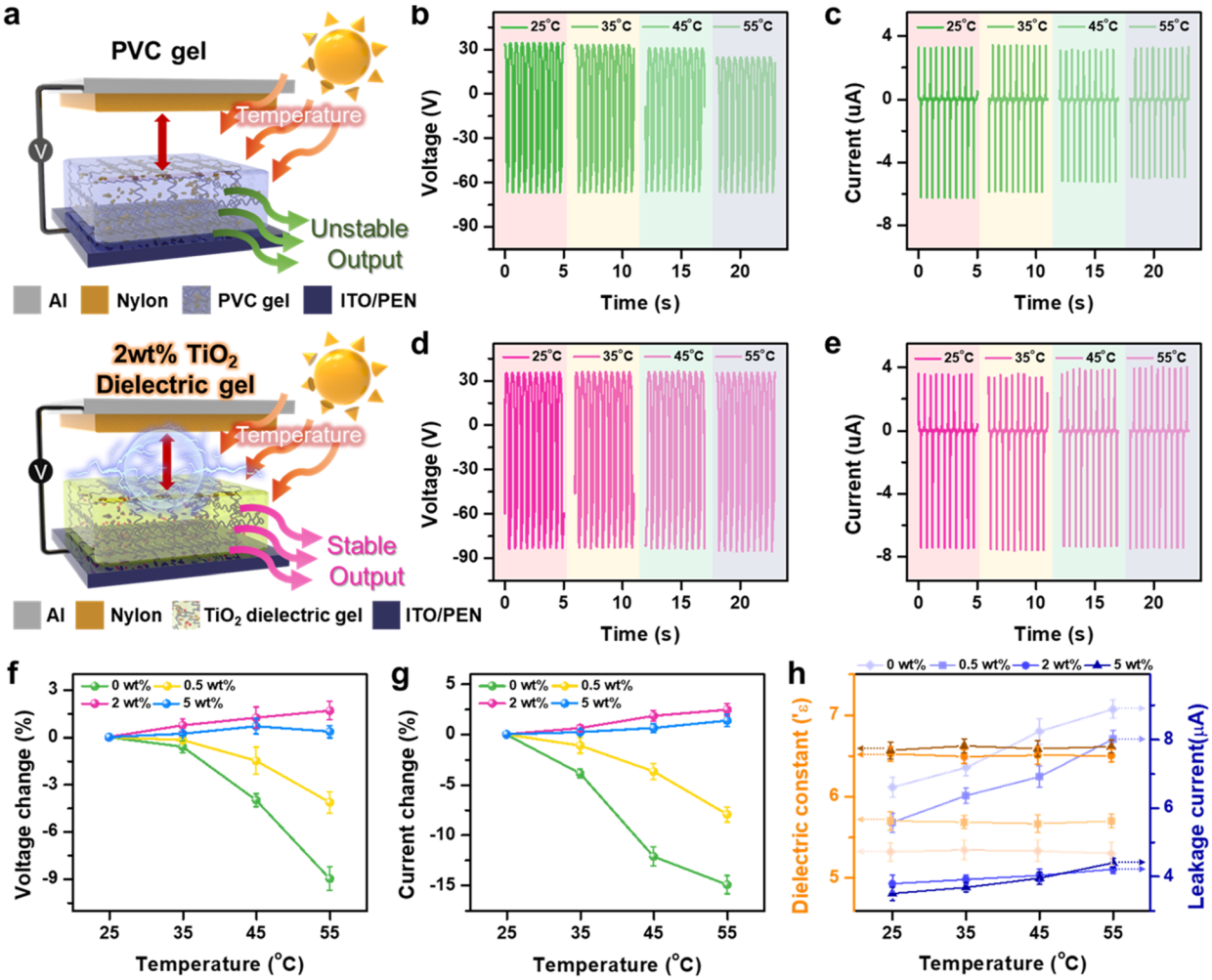

Fig. 3 Reliable energy harvesting based on TiO_2 dielectric gel TENG under elevated thermal conditions. (a) Schematic of PVC gel TENG unstable energy harvesting and 2 wt% dielectric gel TENG reliable energy harvesting under 25 °C to 55 °C thermal conditions. (b) Output voltage and (c) output current of PVC gel TENG under 25 °C to 55 °C thermal conditions. (d) Output voltage and (e) output current of 2 wt% TiO_2 dielectric gel TENG under 25 °C to 55 °C thermal conditions. (f) Output voltage changes and (g) output current changes under different temperature conditions. (h) Dielectric constant and leakage current under the different temperature (25–55 °C).

TiO_2 concentrations (0 wt%, 0.5 wt%) with increasing temperature can be attributed to two main factors: (1) softening of the gel and (2) increased electrical conductivity of the gel. As the temperature rises, the TiO_2 dielectric gel softens, causing greater deformation under the same pressure and reducing the distance between the gel surface and the bottom electrode. Simultaneously, the increased mobility of plasticizers within the gel at higher temperatures leads to higher electrical conductivity (Fig. S14†). These combined effects—reduced surface-to-electrode distance and decreased material resistance—result in significant leakage currents and reduced output performance.[39] In contrast, at higher TiO_2 concentrations (2 wt%, 5 wt%), the superior mechanical modulus and lower leakage current of the gel ensure relatively stable output currents, even under thermal stress. Strong interactions between the TiO_2 nanoparticles and DBA plasticizer restrict the mobility of free DBA molecules, minimizing charge dissipation and enhancing the thermal stability of the TENG output. Thus, the TENG based on the 2 wt% TiO_2 dielectric gel, which shows minimal electrical changes with temperature, can produce stable, high outputs even when exposed to fluctuating outdoor temperature conditions.

3.4 Application: temperature-independent pressure sensor

In the operational dynamics of TENGs, the output increases as greater pressure is applied during the contact-separation process, making TENGs effective for pressure sensing. However, a significant challenge arises when TENG output varies in response to ambient temperature fluctuations, complicating accurate pressure detection. We leveraged the thermal stability of TiO_2 dielectric gel TENGs to develop a pressure sensor that is decoupled from temperature effects (Fig. S15†). The pressure sensor's sensitivity is divided into two pressure ranges: a lower range from 10 kPa to 40 kPa and a higher range from 40 kPa to 100 kPa. Fig. 4a shows that the pressure sensor based on 0 wt% TiO_2 dielectric gel TENG

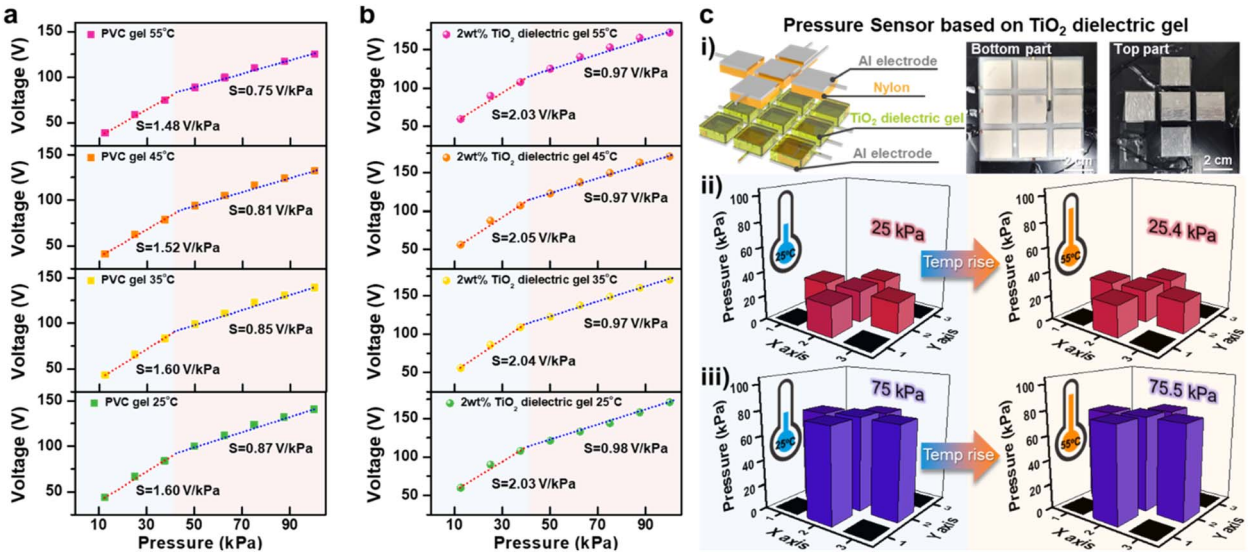

Fig. 4 Temperature-independent pressure sensing based on TiO_2 dielectric gel TENG. (a) PVC gel and (b) 2 wt% TiO_2 dielectric gel TENGs output voltage by different pressure under different temperature (25–55 °C). (c) Temperature-independent pressure sensing application. (c-i) Schematic and photographs of the pressure sensor based on TiO_2 dielectric gel TENG. (c-ii) and (c-iii) Sensing accuracy of the sensor under applied pressure (25 kPa and 75 kPa) at 25 °C and 55 °C.

exhibited sensitivities of 1.60 V kPa^{-1} and 0.87 V kPa^{-1} in the low- and high-pressure ranges, respectively, at 25 °C. However, these sensitivities dropped to 1.48 V kPa^{-1} and 0.75 V kPa^{-1} at 55 °C, demonstrating a decrease with rising temperatures. In contrast, the pressure sensor based on 2 wt% TiO_2 dielectric gel TENG (Fig. 4b) demonstrated superior performance. At 25 °C, the sensitivities were 2.03 V kPa^{-1} in the low-pressure range and 0.98 V kPa^{-1} in the high-pressure range, outperforming the PVC gel. Notably, this sensor maintained nearly constant sensitivities of 2.04 V kPa^{-1}, 2.05 V kPa^{-1}, and 2.03 V kPa^{-1} in the low-pressure range at 35 °C, 45 °C, and 55 °C, respectively, with minimal variation in the high-pressure range (0.98 V kPa^{-1}). This demonstrates its capability to accurately detect pressure regardless of temperature fluctuations. We also tested the output from 2 wt% TiO_2 dielectric gels with varying thicknesses of 50 μm, 250 μm, and 500 μm across a pressure range from 0.5 kPa to 500 kPa (Fig. S16†). We confirmed a detection limit of 0.5 kPa. Additionally, the 500 μm-thick gel not only provided higher sensitivity but could also detect high pressures ranging from 100 kPa to 300 kPa. Response time and retention time are critical for pressure sensors, and the TiO_2 dielectric gel TENG-based pressure sensor demonstrated a response time of less than 3 ms and a retention time of less than 11 ms (Fig. S17†). We fabricated pressure-sensing applications using PVC gel TENG and 2 wt% TiO_2 dielectric gel TENG (Fig. 4c and S18–S20†). The schematic and photographs of the temperature-independent pressure sensing application are shown in Fig. 4c-i. The application consists of a bottom part (2 wt% TiO_2 dielectric gel/Ag electrode) arranged in a 3 × 3 grid of nine sections and a top part (Nylon/Al electrode) in a plus-sign shape. We evaluated the sensor's performance at 25 °C and 55 °C. At 25 °C, the sensor detected an average pressure of 25 kPa based on the output voltage generated in each section when pressure was applied. At 55 °C, the sensor still detected an average pressure of 25.4 kPa, maintaining accurate pressure sensing (Fig. 4c-ii). To verify accuracy at higher pressures, we applied 75 kPa and observed that the sensor detected 75.5 kPa at 55 °C, confirming its functionality as a temperature-independent pressure sensor (Fig. 4c-iii). In contrast, the PVC gel-based pressure sensor detected pressures of 25 kPa, 50 kPa, 75 kPa, and 100 kPa at room temperature. However, at 55 °C, it detected 22.5 kPa, 44.2 kPa, 67.2 kPa, and 88 kPa under the same applied pressures, demonstrating reduced accuracy due to temperature changes (Fig. S18 and S19†). In addition to temperature, humidity is another key factor influencing the performance of TENGs in external environments. We evaluated the output performance of PVC gel and TiO_2 dielectric gel TENGs under varying humidity levels (10–70%). While the output of both TENGs decreased with increasing humidity, the TiO_2 dielectric gel TENG showed a smaller reduction compared to the PVC gel, attributed to the electron-attracting properties of TiO_2 (Fig. S21†).[36]

3.5 Long-term thermal stability in nano-TiO_2 dielectric gels

To evaluate the durability and reliability of TiO_2 dielectric gels, we conducted a long-term thermal stability test by exposing them to a 65 °C oven environment for one week. Fig. 5a shows the rate of DBA weight reduction over time at 65 °C, revealing a decrease from 39% in PVC gel to 26% in 5 wt% TiO_2 dielectric gel. This indicates a concentration-dependent improvement in stability. Fig. 5b presents photographs of the PVC gel and TiO_2 dielectric gels before and after the thermal test. Initially, each sample measured 3 cm in width and 2.8 cm in height. After the thermal test, the PVC gel exhibited the most significant shrinkage due to plasticizer leakage, while the 5 wt% TiO_2 dielectric gel showed the least reduction in size. The PVC gel's

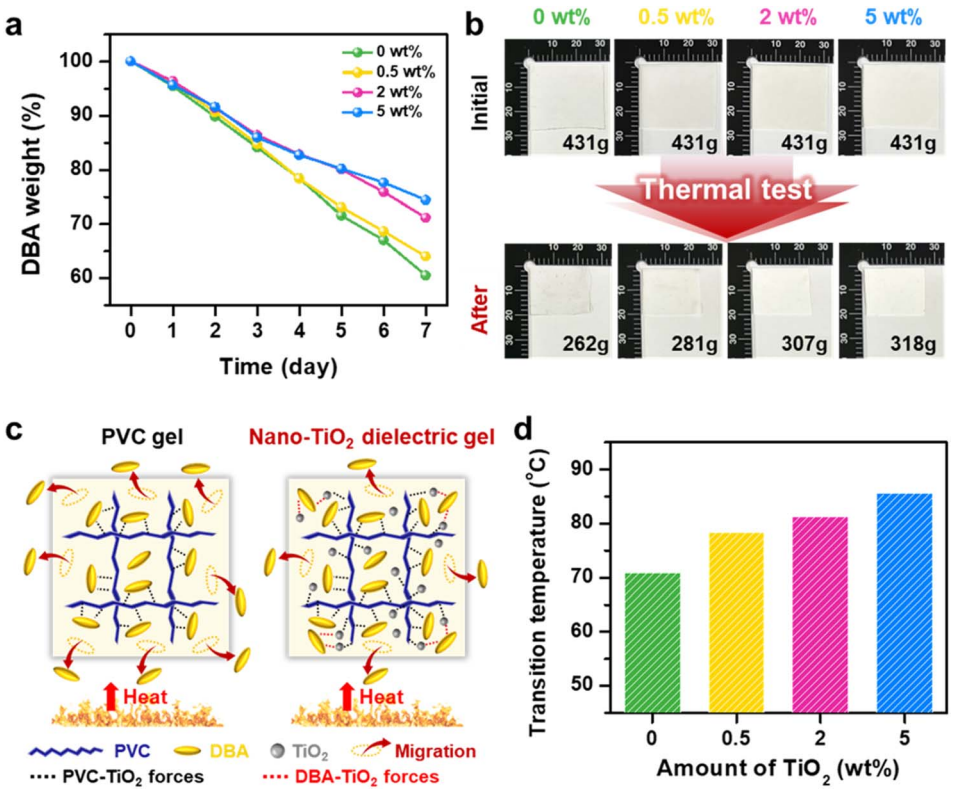

Fig. 5 Long term thermal stability of PVC gel and TiO_2 dielectric gels. (a) DBA weight change of PVC gel and TiO_2 dielectric gels over time at 60 °C. (b) Photographs of PVC gel and TiO_2 dielectric gels before and after 7 days thermal test at 60 °C. (c) Schematic of DBA plasticizer migration to the air by heat energy. (d) DSC transition temperature of PVC gel and TiO_2 dielectric gels.

DBA is physically dispersed, creating free volumes due to the plasticizing effect, which increases the mobility of the plasticizer molecules and accelerates leakage under heat. To enhance thermal stability and reduce plasticizer leakage in PVC gel, TiO_2 nanoparticles were incorporated. These nanoparticles, with their large specific surface area and interactive capabilities with DBA plasticizers, facilitate bonding between the unsaturated free electrons of TiO_2 and the polar regions of DBA molecules. This effectively anchors the plasticizer molecules and limits their mobility within the gel matrix. This mechanism substantially reduces the leakage rate, especially at elevated temperatures, as visually demonstrated in Fig. 5c. Differential Scanning Calorimetry (DSC) data in Fig. 5d further supports these findings, showing that the glass transition temperature of PVC gel increases from 70.9 °C to 85.6 °C with higher TiO_2 content. This underscore enhanced thermal stability due to stronger interfacial interactions within the polymer matrix. Additionally, in the TiO_2 dielectric gels, the C=O peak shifted slightly to the right after annealing, indicating that bonding between DBA and TiO_2 NPs has strengthened and that thermal stability has improved (Fig. S22†). However, while these findings demonstrate the effectiveness of TiO_2 in enhancing thermal stability, we also observed that adding a coupling agent to the TiO_2 dielectric gel, although effective in preventing plasticizer leakage, significantly compromises TENG performance, as shown in Fig. S23.† This underscores the trade-offs between thermal stability and TENG performance, emphasizing the need for future research to optimize this balance for practical applications.

4. Conclusion

This study successfully demonstrated the effectiveness of TiO_2 nanoparticles in improving the thermal stability and electrical performance of polyvinyl chloride (PVC) dielectric gel-based triboelectric nanogenerators (TENGs). By incorporating TiO_2 nanoparticles into the PVC gel, we achieved significant enhancements in the material's dielectric properties, which substantially increased the energy harvesting capabilities of the TENGs. Specifically, the addition of 2 wt% TiO_2 nanoparticles led to a maximum output voltage of 121 V and a current of 11.1 μA, representing a 20% improvement compared to TENGs fabricated solely from PVC gel. Furthermore, the inclusion of TiO_2 nanoparticles effectively mitigated the issue of plasticizer leakage, a common problem in traditional PVC gel TENGs at elevated temperatures. This enhancement not only stabilizes the operational performance of the TENGs but also broadens their applicability across a range of environmental conditions, from 25 °C to 55 °C. The development of a temperature-independent pressure sensor based on this technology marks a significant advancement, offering reliable and consistent performance under varying climatic conditions. This progress paves the way for expanded applications in wearable technology and Internet of Things (IoT) devices.

Data availability

The data supporting this article have been included as part of the ESI.†

Author contributions

Hyosik Park: conceptualization, methodology, visualization, writing – review & editing. Yeonkyeong Ryu: data curation, conceptualization, investigation, writing – original draft. Hyeonseo Joo: validation, investigation. Sujeong Gwak: methodology, visualization. Gbadam Gerald Selasie: formal analysis, validation. Simiao Niu: validation, methodology, formal analysis. Ju-Hyuck Lee: conceptualization, supervision, writing – review & editing. Hyosik Park and Yeonkyeong Ryu contributed equally to this work.

Conflicts of interest

There are no conflicts to declare.

Acknowledgements

This research was supported by the Nano & Material Technology Development Program through the National Research Foundation of Korea (NRF) funded by Ministry of Science and ICT (RS-2024-00451318). This work was supported by the National Research Foundation (RS-2024-00406674) funded by the Ministry of Science and ICT of Korea.

References

1 M. H. Bagheri, A. A. Khan, S. Shahzadi, *et al.*, Advancements and challenges in molecular/hybrid perovskites for piezoelectric nanogenerator application: A comprehensive review, *Nano Energy*, 2023, 109101.
2 Y. Kim, H. Park, Y. Kim, *et al.*, Control of the Biodegradability of Piezoelectric Peptide Nanotubes Integrated with Hydrophobic Porphyrin, *ACS Appl. Mater. Interfaces*, 2022, **14**, 38778–38785.
3 H. Park, Y. Kim, Y. Kim, *et al.*, Self-assembly of unidirectionally polarized piezoelectric peptide nanotubes using environmentally friendly solvents, *Appl. Surf. Sci.*, 2023, **618**, 156588.
4 S. Korkmaz and İ. A. Kariper, Pyroelectric nanogenerators (PyNGs) in converting thermal energy into electrical energy: Fundamentals and current status, *Nano Energy*, 2021, **84**, 105888.
5 G. Prestopino, R. Pezzilli, N. J. Calavita, *et al.*, Layered-Double-Hydroxide (LDH) pyroelectric nanogenerators, *Nano Energy*, 2023, **118**, 109017.
6 H. Ryu and S. W. Kim, Emerging pyroelectric nanogenerators to convert thermal energy into electrical energy, *Small*, 2021, **17**, 1903469.
7 X. Chen, C. Jiang, Y. Song, *et al.*, Integrating hydrovoltaic device with triboelectric nanogenerator to achieve simultaneous energy harvesting from water droplet and vapor, *Nano Energy*, 2022, **100**, 107495.
8 L. Li, M. Hao, X. Yang, *et al.*, Sustainable and flexible hydrovoltaic power generator for wearable sensing electronics, *Nano Energy*, 2020, **72**, 104663.
9 L. Wang, W. Zhang and Y. Deng, Advances and Challenges for Hydrovoltaic Intelligence, *ACS Nano*, 2023, **17**, 14229–14252.
10 T. Cheng, J. Shao and Z. L. Wang, Triboelectric nanogenerators, *Nat. Rev. Methods Primers*, 2023, **3**, 39.
11 D. Choi, Y. Lee, Z.-H. Lin, *et al.*, Recent advances in triboelectric nanogenerators: from technological progress to commercial applications, *ACS Nano*, 2023, **17**, 11087–11219.
12 C. Wu, A. C. Wang, W. Ding, *et al.*, Triboelectric nanogenerator: a foundation of the energy for the new era, *Adv. Energy Mater.*, 2019, **9**, 1802906.
13 G. Yao, L. Xu, X. Cheng, *et al.*, Bioinspired triboelectric nanogenerators as self-powered electronic skin for robotic tactile sensing, *Adv. Funct. Mater.*, 2020, **30**, 1907312.
14 S. Wu, H. Kan, J. Gao, *et al.*, Convolutional Neural Networks-Motivated High-Performance Multi-Functional Electronic Skin for Intelligent Human-Computer Interaction, *Nano Energy*, 2024, **122**, 109313.
15 H. Park, S. J. Oh, D. Kim, *et al.*, Plasticized PVC-gel single layer-based stretchable triboelectric nanogenerator for harvesting mechanical energy and tactile sensing, *Adv. Sci.*, 2022, **9**, 2201070.
16 D. Lu, T. Liu, X. Meng, *et al.*, Wearable triboelectric visual sensors for tactile perception, *Adv. Mater.*, 2023, **35**, 2209117.
17 S. Lu, W. Lei, Q. Wang, *et al.*, A novel approach for weak current signal processing of self-powered sensor based on TENG, *Nano Energy*, 2022, **103**, 107728.
18 M. Salauddin, S. S. Rana, M. Sharifuzzaman, *et al.*, Highly Electronegative V2CTx/Silicone Nanocomposite-Based Serpentine Triboelectric Nanogenerator for Wearable Self-Powered Sensors and Sign Language Interpretation, *Adv. Energy Mater.*, 2023, **13**, 2203812.
19 X. Shi, W. Si, J. Zhu, *et al.*, Boosting the Electrical Performance of PLA-Based Triboelectric Nanogenerators for Sustainable Power Sources and Self-Powered Sensing, *Small*, 2024, **20**, 2307620.
20 H. Joo, S. Gwak, H. Park, *et al.*, Engineering self-healable and biodegradable ionic polyurethane with highly tribopositive behavior, *Nano Energy*, 2024, **126**, 109706.
21 M. Kim, H. Park, M. H. Lee, *et al.*, Stretching-insensitive stretchable and biocompatible triboelectric nanogenerators using plasticized PVC gel and graphene electrode for body-integrated touch sensor, *Nano Energy*, 2023, **107**, 108159.
22 L. Yang, L. Guo, Z. Wang, *et al.*, Stretchable Triboelectric Nanogenerator Based on Liquid Metal with Varying Phases, *Adv. Sci.*, 2024, **11**, 2405792.
23 D. U. Lim, E. J. Lee, J. K. Jang, *et al.*, Ion-Impregnated Intermediate Layer for Enhancing Triboelectric Nanogenerator Performance, *Adv. Funct. Mater.*, 2024, 2401717.

24 Y. Lan, W. Liu, Z. Lv, *et al.*, Liquid-free, tough and transparent ionic conductive elastomers based on nanocellulose for multi-functional sensors and triboelectric nanogenerators, *Nano Energy*, 2024, **129**, 110047.
25 P. Yang, Y. Shi, S. Li, *et al.*, Monitoring the degree of comfort of shoes in-motion using triboelectric pressure sensors with an ultrawide detection range, *ACS Nano*, 2022, **16**, 4654–4665.
26 M. Robiul Islam, O. Faruk, S. S. Rana, *et al.*, Poly-DADMAC Functionalized Polyethylene Oxide Composite Nanofibrous Mat as Highly Positive Material for Triboelectric Nanogenerators and Self-Powered Pressure Sensors, *Adv. Funct. Mater.*, 2024, 2403899.
27 M. Feng, X. Kong, Y. Feng, *et al.*, A New Reversible Thermosensitive Liquid–Solid TENG Based on a P (NIPAM-MMA) Copolymer for Triboelectricity Regulation and Temperature Monitoring, *Small*, 2022, **18**, 2201442.
28 F. Xing, Z. Ou, X. Gao, *et al.*, Harvesting electrical energy from high temperature environment by aerogel nano-covered triboelectric yarns, *Adv. Funct. Mater.*, 2022, **32**, 2205275.
29 J. Schneider, M. Matsuoka, M. Takeuchi, *et al.*, Understanding TiO2 photocatalysis: mechanisms and materials, *Chem. Rev.*, 2014, **114**, 9919–9986.
30 Y. J. Kim, J. Lee, S. Park, *et al.*, Effect of the relative permittivity of oxides on the performance of triboelectric nanogenerators, *RSC Adv.*, 2017, **7**, 49368–49373.
31 A. Gholami, M. Hajian, F. Rafiemanzelat, *et al.*, Plasticized poly (vinyl chloride) composites: influence of different nanofillers as antimigration agents, *J. Appl. Polym. Sci.*, 2015, **132**(42559).
32 M. Viana, V. Soares and N. Mohallem, Synthesis and characterization of TiO_2 nanoparticles, *Ceram. Int.*, 2010, **36**, 2047–2053.
33 B. Yang, Y. Bai and Y. Cao, Effects of inorganic nano-particles on plasticizers migration of flexible PVC, *J. Appl. Polym. Sci.*, 2010, **115**, 2178–2182.
34 C. Zhang, Z. Tang, B. Guo, *et al.*, Concurrently improved dispersion and interfacial interaction in rubber/nanosilica composites *via* efficient hydrosilane functionalization, *Compos. Sci. Technol.*, 2019, **169**, 217–223.
35 Z. H. Lin, G. Cheng, Y. Yang, *et al.*, Triboelectric nanogenerator as an active UV photodetector, *Adv. Funct. Mater.*, 2014, **24**, 2810–2816.
36 H.-W. Park, N. D. Huynh, W. Kim, *et al.*, Effects of embedded TiO_{2-x} nanoparticles on triboelectric nanogenerator performance, *Micromachines*, 2018, **9**, 407.
37 S. Yu, Z. Tang, S. Wu, *et al.*, use of naturally small molecule as an intelligent interfacial modifier for strengthening and toughening silica-filled rubber composite, *Compos. Sci. Technol.*, 2022, **227**, 109624.
38 V. Purcar, V. Rădiţoiu, A. Rădiţoiu, *et al.*, Preparation and characterization of some sol-gel modified silica coatings deposited on polyvinyl chloride (PVC) substrates, *Coatings*, 2020, **11**, 11.
39 D. W. Kim, J. H. Lee, I. You, *et al.*, Adding a stretchable deep-trap interlayer for high-performance stretchable triboelectric nanogenerators, *Nano Energy*, 2018, **50**, 192–200.